A comparison of force computations for modeling fluid - structure interaction problems with the lattice Boltzmann volume penalisation method

Erwan Liberge, Claudine Béghein

Discrete and Continuous Dynamical Systems - Series S

doi:10.3934/dcdss.2023200

A COMPARISON OF FORCE COMPUTATIONS FOR MODELING FLUID - STRUCTURE INTERACTION PROBLEMS WITH THE LATTICE BOLTZMANN VOLUME PENALISATION METHOD

Erwan Liberge* and Claudine Béghein

LaSIE UMR 7356 CNRS, Université de La Rochelle
Avenue Michel Crépeau, 17042 La Rochelle Cedex, France

Abstract. In this article, the capability of the VP-LBM (Volume Penalization - Lattice Boltzmann Method) is explored on new cases whose studied physics is quite different from previous work, and the use of fluid force calculation methods within the VP-LBM framework is discussed. The first method, the momentum exchange method, uses the variation of distribution functions near the fluid-solid interface, while the second, the stress integration method, allows the direct integration of fluid forces on this interface. Applied to the VP-LBM, which involves penalizing the solid in the LBM, these two methods can lead to significantly different results. Tests were carried out to investigate the lift and drag coefficients of a NACA 0012 profile at different angles of attack, Reynolds number 1000, an energy extraction system consisting of a translating and rotating foil, and finally the sedimentation of particles under the effect of gravity in a very low Reynolds number channel.

1. **Introduction.** Computational modeling of fluid-structure interaction (FSI) has remained a challenging area of research in recent decades. Many effective methodologies and algorithms for modeling fluid-structure interaction have evolved in recent years. A classical approach consists in coupling a fluid solver for the Navier-Stokes equations with a structure solver, the fluid solver being obtained by a classical discretization method, such as the finite element or finite volume method. In this paper, we propose to use the Lattice Boltzmann method (LBM) as a fluid solver for FSI simulation.

The LBM has been successfully developed for computational fluid mechanics since the 1990s [5], and appears to be an efficient alternative computational method. Based on the Boltzmann equation, the LBM considers the transport of the probability of finding a particle at a given time, position and mesoscopic velocity. Macroscopic variables are obtained using the moments of the distribution functions. The power of the LBM lies in its programming simplicity and short computation time if the algorithm is solved using graphics processing units (GPUs) [12]. The LBM approaches to solving flows around moving bodies can be classified into two families.

The first concerns Bounce-Back methods and their derivatives. Bounce-Back methods consist in considering that a wall rejects the particle, and, for a moving boundary, in locally changing the macroscopic velocity. For moving bodies, this

2020 *Mathematics Subject Classification.* Primary: 65M99, 74F10; Secondary: 76P05.

Key words and phrases. Lattice Boltzmann method, fluid structure interaction, volume penalization, momentum exchange method, stress integration method.

*Corresponding author: Erwan Liberge.

family can be decomposed into 4 groups as suggested by Krüger et al. [18]. In the first group of methods, the boundary is approximated by a staircase [20]. This method can lead to errors in the case of complex geometries, and for moving boundaries it requires a costly step to update the fluid site and a filling algorithm on nodes that become fluid. The second group concerns methods that use interpolation to impose the exact wall velocity [29, 7]. The results obtained with these methods are more accurate, but have a drawback due to interpolation: the mass is not conserved. The other drawback is the use of a filling algorithm to compute quantities on solid nodes that become fluid after boundary movement. The next group focuses on methods called Partially Saturated Bounce-Back (PSBB) in Kruger *et al.* [18]. The principle is that a network node can be a mixed fluid/solid node. The method, originally proposed by Noble and Torczynski [23], involves modifying the collision operator by introducing a solid volume fraction. Finally, the collision operator is a mixture of the classical collision operator and the Bounce-Back method. The major drawback of this method is the difficulty of calculating the solid volume fraction for each node in the network. This limits the field of application of this method to stationary bodies. Krüger et al. propose a final group of methods based on the extrapolation of distribution functions for fluid nodes located near the boundary.

The second family is that of immersed boundary (IB) methods for LBM [13] which consists in modeling the effect of the boundary by adding nodal forces in the vicinity of the boundary, in the fluid flow solver. The main drawback of IB-LBM is that nodal forces use a penalty factor, and hydrodynamic forces and torques depend on this factor for rigid bodies. The direct forcing scheme [11] cancels this disadvantage, but it requires solving the Boltzmann equation twice per time step. Wang et al. [26] propose an alternative approach using a Lattice Boltzmann Flux Solver (LBFS), whose formulation is not efficient for a GPU implementation.

In previous papers [2, 3, 4], we proposed coupling the volume penalization (VP) method [1] and the LBM (VP-LBM). The volume penalization method consists in extending the Navier-Stokes equations to the whole domain (fluid and solid) and adding a volume penalization term to account for structure. This approach can be seen as a cross between the partially saturated rebound method (PSBB) and the immersed boundary method (IB). However, the volume penalty method does not require the costly calculation of the solid fraction near the solid interface as in PSBB methods, and the difference with IB methods is that the VP method uses a volume force, instead of local forces on Lagrangian markers. The capability of penalty methods for fluid-structure interaction problems in a finite element framework has been demonstrated by Destuynder *et al.* [8]. In earlier work, Benamour *et al.* [2, 3] showed that VP-LBM gives good results for fixed bodies. In [4], the method was successfully tested for moving boundaries and a real case of fluid-structure interaction (FSI). In these earlier works, the momentum exchange (ME) method was used to calculate fluid forces and, although the results were validated, spurious oscillations could be observed in the case of fluid-structure interaction on lift and drag coefficients. In this article, we propose first to present the performance of the VP-LBM approach for new cases for which the physics of fluid flow is radically different from previous work, and then to compare the accuracy of the ME method and the other well-known method for calculating forces in LBM, the stress integration method (SI) on these cases. The first case is the study of a NACA 0012 airfoil with angles of attack from 0° to 28° at Reynolds number 1000, the objective here is to capture the stall phenomena, the second is the imposed displacement of

a NACA 0015 which is part of a power extractor, and the last is the sedimentation of particles under the effect of gravity in a channel at very low Reynolds number.

The theoretical background is presented in the next section. This section deals with the Lattice Boltzmann method, and more specifically with the two-relaxation-time (TRT) approach, volume penalization and the combination of these two methods. Next, the momentum exchange (ME) and stress integration (SI) methods are introduced. The final section presents applications computed on a GPU device. For the first case tested, the lift and drag coefficients of a NACA 0012 profile at different angles of attack, Reynolds number 1000, obtained with ME and SI are compared with literature data. The second example deals with a foil oscillating in translation and rotation, leading to a disturbed fluid flow configuration. The next case explores the ability of the VP-LBM method to model a very low Reynolds number phenomenon represented here by the sedimentation of particles under the effect of gravity in a channel.

2. Governing equations.

In this section, the numerical models are described. The following notations are used: ρ and $\mathbf{u}$ are macroscopic density and velocity, and boldface type designates vectors.

2.1. Volume penalization.

Let's consider a fluid domain Ω_f, a solid domain Ω_s, Γ the fluid-solid interface, and let's denote $\Omega = \Omega_f \cup \Omega_s \cup \Gamma$. The Volume Penalization (VP) method consists in extending the Navier-Stokes equations to the entire Ω domain, and considering the solid domain as a porous medium with very low permeability. The method was introduced by Angot et al.[1] and already applied to macroscopic equations for moving bodies [16]. The low permeability of the solid domain is modeled using a penalization factor, allowing the desired boundary conditions to be imposed naturally at the fluid-solid interface. With this method, the incompressible Navier-Stokes equations are written as follows:

$$\begin{aligned} &\nabla \cdot \mathbf{u} = 0 \\ &\frac{\partial \mathbf{u}}{\partial t} + \mathbf{u} \cdot \nabla \mathbf{u} = -\frac{1}{\rho}\nabla p + \nu \nabla^2 \mathbf{u} - \frac{\chi_s}{\eta}\left(\mathbf{u} - \mathbf{u}_s\right) \end{aligned} \tag{1}$$

where

$$\chi_s\left(\mathbf{x}, t\right) = \begin{cases} 1 & \text{if } \mathbf{x} \in \Omega_s\left(t\right) \\ 0 & \text{otherwise} \end{cases} \quad ; \qquad \eta \ll 1 \ \text{ penalization factor} \tag{2}$$

$\mathbf{u}$ represents the velocity field, p is the pressure field, ρ and ν are the density and viscosity of the fluid. $\mathbf{F} = \dfrac{\chi_s}{\eta}\left(\mathbf{u} - \mathbf{u}_s\right)$ is the penalization term, and $\mathbf{u}_s$ is the velocity field in the solid domain.

2.2. Lattice Boltzmann method.

Based on the Boltzmann equation (equation (3)) proposed in the context of the kinetic theory of gas by L. Boltzmann in 1870, the Boltzmann lattice method has been successfully used to model fluid flow since the 1990s.

$$\frac{\partial f}{\partial t} + \mathbf{c} \cdot \nabla_x f = \Omega\left(f\right) \tag{3}$$

This equation models the transport of $f\left(\mathbf{x}, t, \mathbf{c}\right)$, a probability density function of particles with velocity $\mathbf{c}$ at location $\mathbf{x}$ and time t. $\Omega\left(f\right)$ is the collision operator. The link between the Boltzmann equation and the Navier-Stokes equations is well known since the Chapmann-Enskog expansion proposed in 1915.

The lattice Boltzmann method considers the discretization of the equation (3) in space and velocity, and leads to the following discretized equations:

$$f_\alpha\left(\mathbf{x}+\mathbf{c}_\alpha\triangle t, t+\triangle t\right)-f_\alpha\left(\mathbf{x},t\right)=\Omega_\alpha\left(f\right)+\triangle t F_\alpha \tag{4}$$

where $f_\alpha\left(\mathbf{x},t\right)=f\left(\mathbf{x},\mathbf{c}_\alpha,t\right)$, F_α is a forcing term related to the discrete velocity $\mathbf{c}_\alpha$ [15].

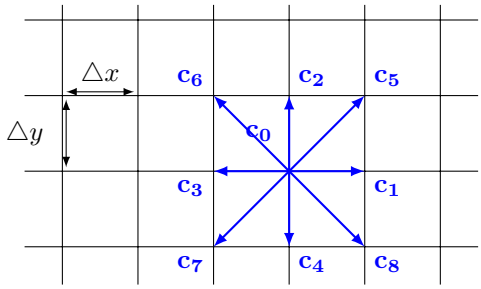

FIGURE 1. Discrete velocities of the D2Q9 model

$$\mathbf{c}_\alpha=\begin{cases}(0,0) & \alpha=0\\ \left(\cos\left(\left(\alpha-1\right)\frac{\pi}{2}\right),\sin\left(\left(\alpha-1\right)\frac{\pi}{2}\right)\right)c & \alpha=1,2,3,4\\ \left(\cos\left(\left(2\alpha-9\right)\frac{\pi}{4}\right),\sin\left(\left(2\alpha-9\right)\frac{\pi}{4}\right)\right)\sqrt{2}c & \alpha=5,6,7,8\end{cases} \tag{5}$$

Where $c=\dfrac{\triangle x}{\triangle t}$. We generally choose $\triangle x=\triangle y=\triangle t=1$.

The first model proposed by Bhatnagar et al. [6] is the BGK model which is based on a linear collision operator with a single relaxation time:

$$\Omega_\alpha\left(f\right)=-\frac{1}{\tau}\left(f_\alpha\left(\mathbf{x},t\right)-f_\alpha^{\mathrm{eq}}\left(\mathbf{x},t\right)\right) \tag{6}$$

where f^{eq} is the equilibrium function,

$$f_\alpha^{\mathrm{eq}}=\omega_\alpha\rho\left(1+\frac{\mathbf{c}_\alpha\cdot\mathbf{u}}{c_s^2}+\frac{\mathbf{uu}:\left(\mathbf{c}_\alpha\mathbf{c}_\alpha-c_s^2 I\right)}{2c_s^4}\right), \tag{7}$$

$\omega_\alpha=\{4/9,1/9,1/9,1/9,1/9,1/36,1/36,1/36,1/36\}$, $c_s=\dfrac{c}{\sqrt{3}}$ and τ is the non-dimensional relaxation time which is related to the fluid viscosity as follows.

$$\nu=c_s^2\triangle t\left(\tau-\frac{1}{2}\right) \tag{8}$$

In order to increase the stability, approaches using multiple relaxation times have been proposed [9, 18]. In this work, the Two Relaxation Times (TRT) method is used.

We denote $\mathbf{c}_\alpha$ the discrete velocity in the α direction and $\mathbf{c}_{\bar{\alpha}}=-\mathbf{c}_\alpha$ the discrete velocity in the opposite $\bar{\alpha}$ direction.

The TRT method consists of introducing modified positive and negative distribution functions:

$$f_\alpha^+=\frac{f_\alpha+f_{\bar{\alpha}}}{2}\ ,\ f_\alpha^-=\frac{f_\alpha-f_{\bar{\alpha}}}{2}. \tag{9}$$

In the same way, $f_\alpha^{eq\ +}$ and $f_\alpha^{eq\ -}$ are defined.

This leads to the following discretized scheme :

$$\begin{aligned} & f_\alpha\left(\mathbf{x}+\mathbf{c}_\alpha \Delta t, t+\Delta t\right)-f_\alpha(\mathbf{x}, t) \\ & =-\frac{\Delta t}{\tau^{+}}\left(f_\alpha^{+}(\mathbf{x}, t)-f_\alpha^{eq\ +}(\mathbf{x}, t)\right) \\ & \quad-\frac{\Delta t}{\tau^{-}}\left(f_\alpha^{-}(\mathbf{x}, t)-f_\alpha^{eq\ -}(\mathbf{x}, t)\right)+\left(1-\frac{\Delta t}{2 \tau^{+}}\right) F_\alpha, \end{aligned} \tag{10}$$

where τ^+ is the relaxation time linked with the non-dimensional viscosity ν according to:

$$\nu=c_s^2 \triangle t\left(\tau^{+}-\frac{1}{2}\right). \tag{11}$$

The relaxation time τ^- is obtained as follows:

$$\tau^{-}=\frac{\Delta t\ \Lambda}{\tau^{+}-\frac{1}{2}}+\frac{1}{2}, \tag{12}$$

In this work, we choose $\Lambda=\frac{1}{6}$, because of the better stability we obtained with this value.

Finally, macroscopic quantities arecomputed according to the following expressions:

$$\rho=\sum_\alpha f_\alpha \qquad \rho \boldsymbol{u}=\sum_\alpha \mathbf{c}_\alpha f_\alpha+\frac{\triangle t}{2} \rho \mathbf{F} \tag{13}$$

In the present approach, the volume penalization term is added:

$$\rho \mathbf{u}=\sum_\alpha \mathbf{c}_\alpha f_\alpha-\frac{\triangle t}{2} \rho \frac{\chi_s}{\eta}\left(\mathbf{u}-\mathbf{u}_s\right) \tag{14}$$

To avoid instabilities, the term including $\mathbf{u}$ in the penalization force is moved to the left hand side of equation (14)

$$\rho\left(1+\frac{\triangle t}{2} \frac{\chi_s}{\eta}\right) \mathbf{u}=\sum_\alpha \mathbf{c}_\alpha f_\alpha+\frac{\triangle t}{2} \rho \frac{\chi_s}{\eta} \mathbf{u}_s \tag{15}$$

This leads to the modified update step for computing the macroscopic velocity field:

$$\mathbf{u}=\frac{\sum_\alpha \mathbf{c}_\alpha f_\alpha+\frac{\triangle t}{2} \frac{\chi_s}{\eta} \rho \mathbf{u}_s}{\rho+\frac{\triangle t}{2} \frac{\chi_s}{\eta} \rho} \tag{16}$$

In the fluid domain, where $\chi_s=0$, the classical LBM equation is obtained, while in the solid domain, where $\chi_s=1$, the equation (16) forces the velocity field to approach $\mathbf{u}_s$.

2.3. **Fluid forces computation.** Angot *et al.* [1] proposed in the context of an integral formulation of the volume penalization problem to compute the fluid forces with the following formula:

$$\boldsymbol{\mathcal{F}}_f=\lim_{\eta \longrightarrow \infty} \int_{\Omega_s} \mathbf{u}-\mathbf{u}_s d \Omega \tag{17}$$

The formula (17) works with finite element or finite volume methods, but fails in our calculation tests. We present below the two classical methods used in the LBM to calculate fluid forces.

2.3.1. *Momentum Exchange Method (ME).* The fluid forces are computed with the Momentum Exchange method (ME) proposed by Wen at al.[27]. We denote $\mathbf{x}_f$ a boundary node in the fluid domain and $\mathbf{x}_s$ the image of this boundary node across the solid interface by a lattice velocity $\mathbf{c}_\alpha$, also called the incoming velocity (see figure 2). The point of intersection between the fluid-solid interface and the link $\mathbf{x}_f - \mathbf{x}_s$ is $\mathbf{x}_\Gamma$, and the outgoing network velocity is denoted $\mathbf{c}_{\overline{\alpha}} = -\mathbf{c}_\alpha$.

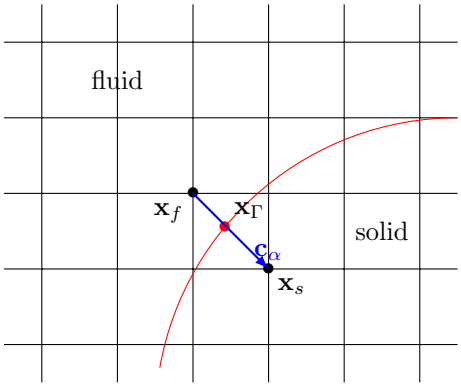

FIGURE 2. Curved interface on a square lattice: example of a fluid boundary node $\mathbf{x}_f$, its image in the solid domain $\mathbf{x}_s$, and the intersection point $\mathbf{x}_\Gamma$ located on the interface

The local force at $\mathbf{x}_\Gamma$ is computed using the following expression:

$$\mathbf{F}(\mathbf{x}_\Gamma) = (\mathbf{c}_\alpha - \mathbf{u}_\Gamma)\,\tilde{f}_\alpha(\mathbf{x}_f) - (\mathbf{c}_{\overline{\alpha}} - \mathbf{u}_\Gamma)\,\tilde{f}_{\overline{\alpha}}(\mathbf{x}_s)\,, \tag{18}$$

and the total fluid force acting on the solid domain is:

$$\boldsymbol{\mathcal{F}}_f = \sum \mathbf{F}(\mathbf{x}_\Gamma) \tag{19}$$

The torque is obtained with

$$\boldsymbol{\mathcal{T}}_f = \sum (\mathbf{x}_\Gamma - \mathbf{x}_G) \times \mathbf{F}(\mathbf{x}_\Gamma)\,, \tag{20}$$

with $\mathbf{x}_G$ the coordinates of the body's center of gravity. A simple way to implement the ME method is to use the characteristic function and calculate on the nodes around the solid:

$$\mathbf{F}(\mathbf{x}_\Gamma) * (\chi_s(\mathbf{x}_s) * (1 - \chi_s(\mathbf{x}_f))$$

This method avoids the need to search explicitly for the point of intersection $\mathbf{x}_\Gamma$.

Giovacchini and Ortiz [14] have shown that the ME does not depend on how the solid domain boundary conditions are implemented.

2.3.2. *Stress Integration Method (SIM).* This method is more intuitive in computational fluid dynamics, and consists of integrating the stress tensor of the fluid on the structure:

$$\boldsymbol{\mathcal{F}}_f = \int_{\partial\Omega_s} \sigma \cdot \mathbf{n} dS \text{ and } \boldsymbol{\mathcal{T}}_f = \int_{\partial\Omega_s} \mathbf{r} \times \sigma \cdot \mathbf{n} dS \tag{21}$$

with

$$\begin{aligned} \sigma &= -pI_d + \nu\left(\nabla\mathbf{u} + (\nabla\mathbf{u})^T\right) \\ &= -\rho c_s^2 I_d - \left(1 - \frac{1}{2\tau}\right)\left(\sum_\alpha \mathbf{c}_\alpha \otimes \mathbf{c}_\alpha\,(f_\alpha - f_\alpha^{eq})\right) \end{aligned} \tag{22}$$

and $\mathbf{n}$ is the external unit normal vector to the solid interface.

The f_α are extrapolated from the nearest point in the direction concerned (close to $\mathbf{n}$) in the fluid domain to the $\mathbf{x}_i$ integration points located on the surface. Finally, equation (21) becomes:

$$\boldsymbol{\mathcal{F}}_f = \sum_i S_i \sigma(\mathbf{x}_i) \cdot \mathbf{n}_i \tag{23}$$

S_i and $\mathbf{n}_i$ are the integration surface and the exterior normal at the integration point $\mathbf{x}_i$.

3. Applications.

All computations were performed on a NVIDIA QUADRO P500 GPU card, using a CUDA implementation. A penalization factor value $\eta = 10^{-6}$ was chosen for all cases[1].

In the following, l.u. denotes lattice length units and t.s. denotes lattice time units.

3.1. NACA airfoil.

The first application is the study of the NACA 0012 airfoil with different values of angle of attack at Reynolds number 1000. This case is well documented in the literature, and the different ME or SI results for VP-LBM are compared with those obtained by [10, 19, 22].

Liu *et al.* [22] uses the finite element method combined with fine meshing to obtain accurate numerical results. Kurtulus [19] offers a very comprehensive study, using the finite volume method and extensive data for comparison. Di Illio *et al.* [10] combines the standard LBM method with an unstructured finite volume formulation in the so-called hybrid Boltzmann lattice method. They used an overlap between a standard LBM approach on the whole domain and an unstructured grid model adapted to the body where a finite volume Boltzmann formulation is applied. This approach produced highly accurate results close to the body. However, no information was given on the calculation of fluid forces. This appears to be a stress integration method, as the macroscopic values are taken directly from the mesh fitted to the body.

The figure 3 represents the computational domain. Let C be the chord of the

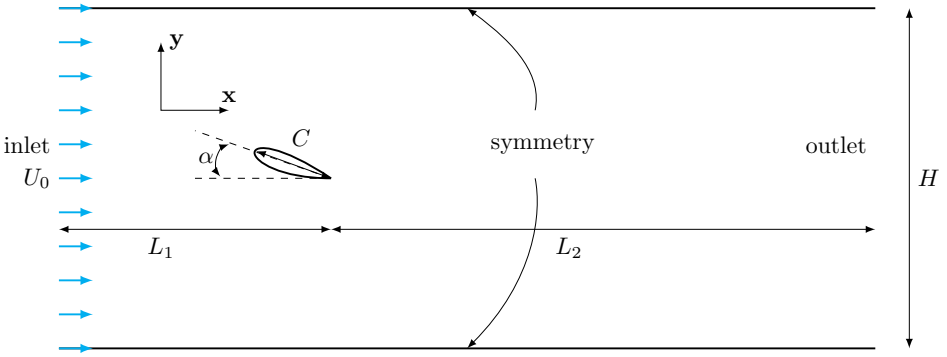

FIGURE 3. Scheme of the computational domain around the NACA airfoil

NACA 0012. The airfoil is placed at $4C$ from the inlet and $9C$ from the outlet. The height of the computational domain is $7C$, and the NACA is $3.5C$ from the bottom.

[1]No difference was observed for a value below 10^{-3}. 10^{-6} is a value that guarantees that the penalization term dominates the other terms of the calculation in the solid domain.

A constant velocity profile was imposed at the inlet using the classical halfway bounce back method, and the flow boundary condition at the outlet was modeled using the convection condition [28]. This condition reduces the distance between the aerodynamic profile and the extreme limit of the computational domain downstream of the immersed body. Boundary symmetry conditions ($\mathbf{u} \cdot \mathbf{n} = 0$) were imposed on the other boundaries.

The computations were performed using the following parameters (in lattice units):

$$C = 278, \quad U_0 = 0.0599, \quad \tau = 0.55$$

Note that τ is close to the stability limit for LBM, but this makes it possible to reduce C and therefore the size of the computational problem as well as the computation time. Di Illio *et al.* [10] used 512 nodes in the string, and a larger computational domain. However, our interest in VP-LBM solved in CUDA being computation time, we are trying to get a good qualitative result without resorting to overly expensive computational resources. That is why this set of parameters was used.

For the Stress Integration method, 849 integrations points have been used. Note that the number of integration points was chosen arbitrarily. Increasing their number increases the accuracy of the calculation, but not significantly in this case.

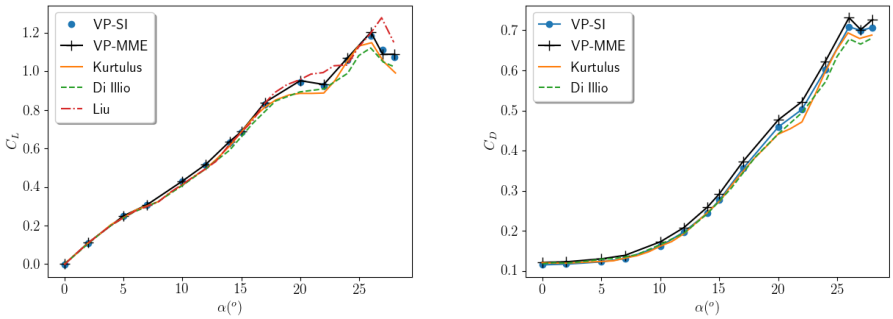

(a) Lift coefficient (b) Drag coefficient

FIGURE 4. Lift and Drag coefficient versus angle. The VP-LBM's results computed with Stress Integration and Momentum Exchange methods are compared with those in the literature

The drag and lift coefficients are plotted in figure 4. The VP-LBM gives a good prediction of these values compared with the literature.

For $\alpha \leq 8°$ a steady solution has been obtained, leading to a slight increase in drag. Then, up to 24°, a periodic vortex shedding is observed (figures (5(b)) and (5(c)). During this phase, the increase in drag and lift is regular. An irregularity in the lift coefficient appears at 26°. This stall phenomena is well captured with the VP-LBM approach, and the numerical value is also well computed with ME as well SI.

Note that the values obtained here are slightly higher than those obtained by [19] and Di Illio *et al.* [10], but lower than those obtained by Liu *et al.*[22]. As our results are close to those of Liu *et al.* [22] and Di Illio [10], they can be considered

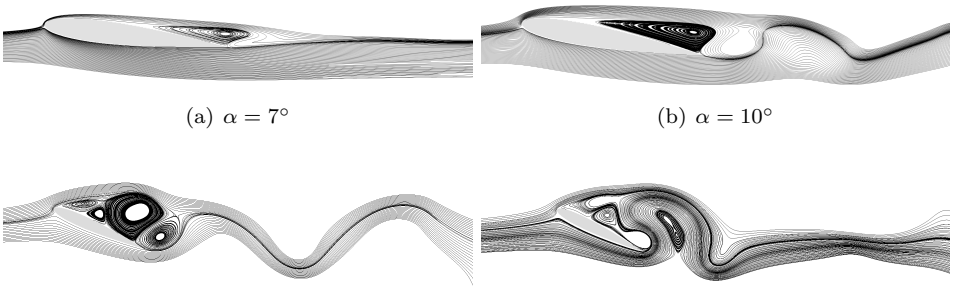

(a) $\alpha = 7°$ (b) $\alpha = 10°$

(c) $\alpha = 24°$ (d) $\alpha = 26°$

FIGURE 5. Streamlines around NACA 0012 for various angles

validated. If we consider that the work of Di Illio *et al.* [10] is the reference, because a finer mesh is used, the Stress Integration method gives better results than the Momentum Exchange method. SI provides a better approximation of the surface, with a direct discretization of the solid boundary, and a true outward normal, while ME used a staircase approximation. The limit of SI, which is an extrapolation of the distribution values on the boundary, does not seem to have any consequences in these cases.

Lift forces are fairly similar, with neither ME nor SI affecting the results. Drag was slightly overestimated with ME, probably due to the approximation of the computational boundary induced by this method.

3.2. **Oscillating foil.** The second example concerns a power extraction system presented by Kinsey and Dumas [17]. The system consists of a NACA 0015 foil whose translational and rotational displacement is imposed. The vertical displacement $y(t)$ and the rotation $\theta(t)$ of the foil are imposed according to the following expressions:

$$y(t) = Y_0 \sin(\gamma t + \phi) \quad \text{and} \quad \alpha(t) = \alpha_0 \sin(\gamma t) \tag{24}$$

The capacity of the VP-LBM method was tested for the physical parameters $H_0 = C, \alpha_0 = 76.33$ deg, $Re = 1100$, with the following LBM parameters (in lattice units): $C = 459$, $U_O = 0.039941$ and $\tau = 0.55$.

In the figure 6 the power coefficient c_p, which represents the instantaneous power extracted from the flow, over a period of oscillation T is plotted and compared. The c_p coefficient makes it possible to concatenate the lift and torque coefficients into a single coefficient:

$$c_p(t) = \frac{\boldsymbol{\mathcal{F}}_f(t) \cdot \boldsymbol{U}(t) + \boldsymbol{\mathcal{T}}_f(t) \cdot \boldsymbol{\Omega}(t)}{\frac{1}{2}\rho U_0 C}, \tag{25}$$

with $\boldsymbol{U}$ and $\boldsymbol{\Omega}$ representing the velocity of the NACA's center of gravity and the angular velocity of pitch.

The evolution of power due to the significant variation in oscillation angle is well captured, and the power extracted by the fluid calculated by the VP-LBM method, whatever the method used to calculate the fluid forces, is as good as the literature reference.

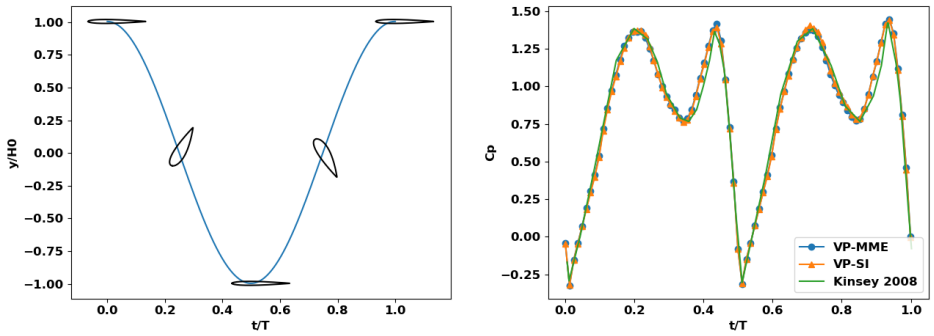

(a) Imposed displacement (b) Drag coefficient

FIGURE 6. Comparison of the power extractor coefficient (equation (25)) obtained using the VP-LBM method and the literature reference

Figures 7 and 8 show the fluid patterns for two foil angles during the descending phase. Figure 7 shows the vorticity field for the maximum foil angle. The vortices previously detached from the foil and descending into the fluid flow are well captured, even the three lowest amplitude vortices in the bottom right of figure 7(b).

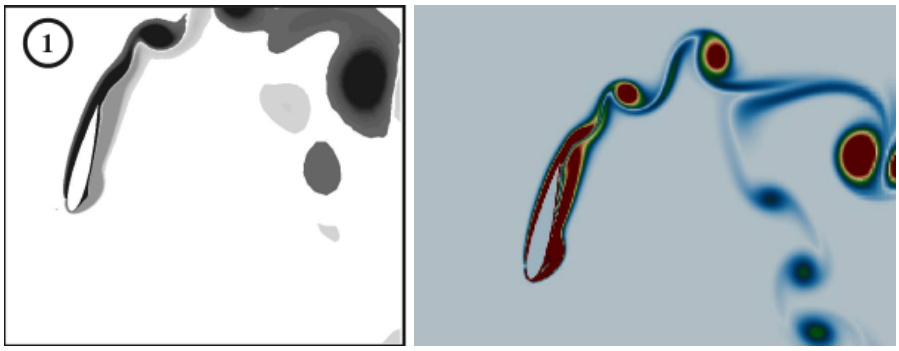

(a) Literature reference (b) VP-LBM result

FIGURE 7. Comparison of the vorticity field obtained by [17] and by the LBM-VP for $t/T = 0.25$

Figure 8 shows the fluid flow for the second peak of the CP maximum on figure 6 for a dimensionless time around $t/T = 0.45$. Two large vortices under the NACA will escape, and the small vortices in the wake of the foil are the same on both figures 8(a) and 8(b).

The VP-LBM method proved effective in this case to capture the complexity of fluid flow induced by the large translational and rotational displacement of a NACA 0015. The two methods used to calculate fluid forces give similar results in terms of power extraction coefficients.

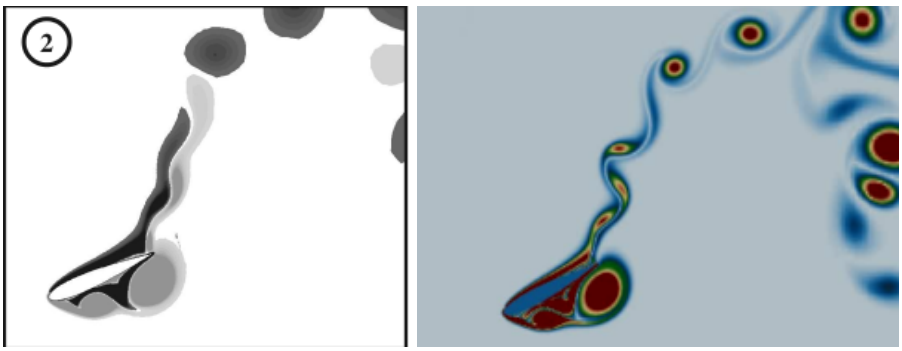

(a) Literature reference (b) VP-LBM result

FIGURE 8. Comparison of the vorticity field obtained by [17] and by the LBM-VP for $t/T = 0.45$

3.3. **Sedimentation of a particle under gravity.** The next case concerns the sedimentation of a particle under the effect of gravity in an infinite channel (figure 9) for non-centered configurations. This problem has been widely used for model validation and is very useful for testing the ability of a method to capture complex trajectories at very low Reynolds numbers [25, 24, 27, 21]. Indeed, at very low Reynolds numbers, numerical noise cannot be hidden by a large average that could cover it.

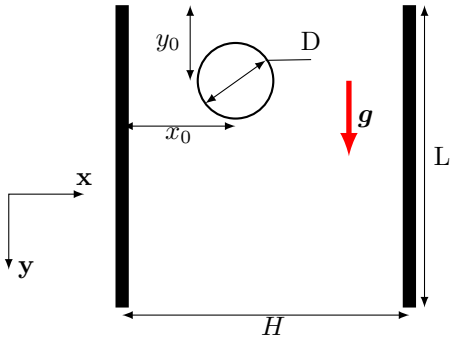

FIGURE 9. Scheme of particle sedimentation

A circular particle of diameter D falls by gravity $\boldsymbol{g}$ into a fluid of density ρ in a vertical channel of width H. In the initial state, the particle is at a distance x_0 from the left wall, a distance y_0 from the top of the channel and the velocity of the particle is equal to zero. In this case, the displacement of the particle can be described using the equations (26) and (27):

$$m\frac{d^2\mathbf{x}_G}{dt^2} = \boldsymbol{\mathcal{F}}_f + m\left(1 - \frac{\rho}{\rho_s}\right)\boldsymbol{g} \tag{26}$$

$$I\frac{d^2\boldsymbol{\theta}}{dt^2} = \boldsymbol{\mathcal{T}}_f \tag{27}$$

where ρ denotes the fluid density, ρ_s the solid density and m the particle mass. The last term of the equation (26) represents the weight and buoyancy (Archimedes' principle) acting on the particle.

For small Reynolds numbers and a large non dimensional width $\tilde{H} = \dfrac{H}{D}$, the particle reaches a steady state.

The following case deals with a particle whose initial position is not at the center of the channel ($x_0 = 0.75D$). The properties of the fluid are $\rho = 1\ \mathrm{g \cdot cm^{-3}}$, and $\mu = 0.1\ \mathrm{g \cdot cm^{-1} \cdot s^{-1}}$ and the physical problem concerns a particle of diameter $D = 0.1$ cm. Four mass ratio $\rho_r = \dfrac{\rho_s}{\rho_f} = 1.0015, 1.003, 1.0015$ and 1.03 and $\|\boldsymbol{g}\| = 980\ \mathrm{cm \cdot s^{-2}}$ are used. The Reynolds numbers based on the final velocity of the particle are, respectively, $\mathrm{Re} = 0.52, 1.03, 3.23$ and 8.33.

For the LBM computations the cylinder diameter was 26 l.u., the same value used in the literature [24], the relaxation time was $\tau = 0.6$. No-slip boundary conditions were imposed on the left and right walls. A zero velocity boundary condition was applied at the inlet (top of the channel) and free flow conditions were applied at the outlet (bottom). A large value of L was chosen, so that the inlet and the outlet do not influence the behavior of the particle.

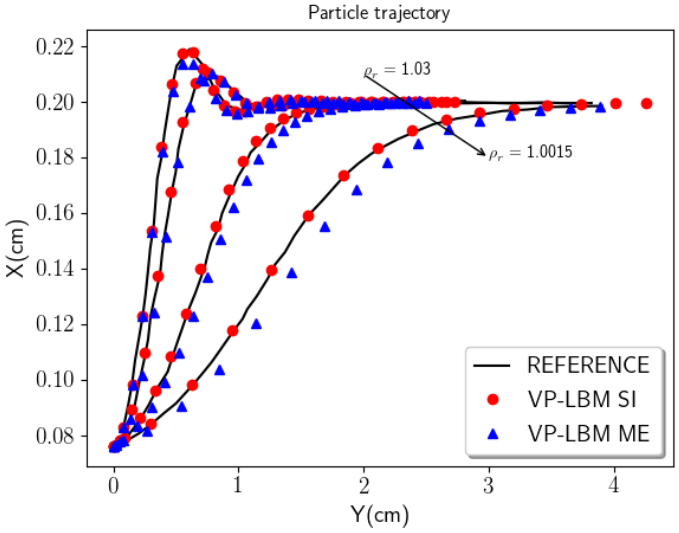

FIGURE 10. Results obtained using the VP-LBM approach and compared with Tao et al's results [24]

The particle trajectory for each mass ratio is plotted in figure 10, and compared with the reference results of the literature [24, 21]. In order to facilitate the reading of the figure, only a few points for each trajectory have been plotted. First of all, it can be noted that the VP-LBM method, coupled with the Stress Integration method gives for each case a good behavior of the particle. The results are similar to those obtained with the UIBB and the literature. This is not what is observed for VP-LBM coupled with Momentum Exchange. The trajectory is almost correct for a high mass ratio, although a small difference can be observed around $t = 0.5$s

for $\rho_r = 1.03$, and the error increases as the mass ratio (i.e the Reynolds number) decreases. Our analysis is that for small mass ratio, the fluid forces are very small, and a small error has a greater significance in the behavior of the particle than for a larger mass ratio. The lack of accuracy of the fluid solid interface has a great consequence here. Extrapolating f_α to the fluid-structure interface in the Stress Integration method not only improves the calculation of fluid forces, but also smoothes out f_α oscillations. The momentum exchange method is affected by the spurious oscillation of f_α values when a solid node becomes solid. This phenomenon has already been observed in the two previous cases, but the amplitudes of the spurious oscillations are too small in relation to the amplitude of the signal, so they are not visible.

Figures 11 show the rotational velocity for the smallest and largest mass ratio. For $\rho_r = 1.0015$ (figure 11(a)) spurious oscillations are observed with ME. Even if the average follows the reference solutions, these oscillations lead to particle deviation from the reference trajectory. In the figure 11(b), oscillations are smaller, but even if the solution is close to the reference one, the Stress Integration gives better results. This phenomenon is well known in ME for moving boundaries. Indeed, as the solid moves, the number of $\mathbf{x}_\Gamma$ points in equations (19) and (20) can change, which can lead to oscillations in the total forces.

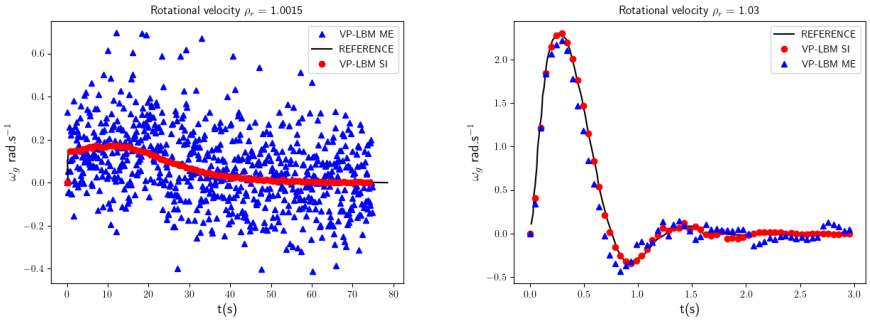

(a) $\rho_r = 1.0015$ (b) $\rho_r = 1.03$

FIGURE 11. Rotational velocity obtained using the VP-LBM approach and compared with reference's results [24, 21]

Figures 12 and 13 show the fluid velocity and the vorticity field around the particle at four different times. The dynamics of the flow field and the particle can be analyzed using the velocity magnitude and the vorticity. The particle first moves to the right and rotates in a positive direction. This is followed by a brief oscillation around the center line of the channel and, finally, the particle remains in the middle of the channel with a constant velocity.

This example shows that the VP-LBM method is capable of predicting a complex trajectory for a real case of fluid-structure interaction at a very low Reynolds number.

4. **Conclusion.** The volume penalization method coupled to the Boltzmann lattice method (VP-LBM) was successfully applied to three cases of different complexity. Available methods for calculating fluid loads were also discussed. The VP-LBM

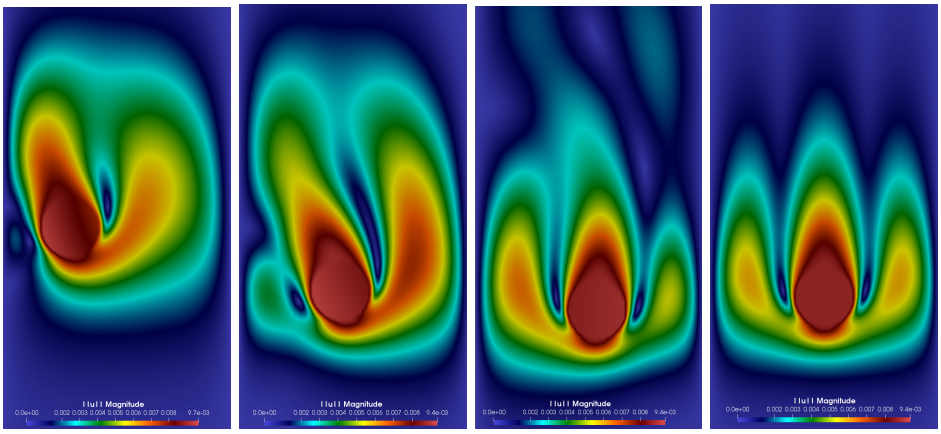

(a) t = 0.4 s (b) t = 0.6 s (c) t = 1.0 s (d) t = 3.0 s

FIGURE 12. Fluid velocity magnitude at times t=0.4, 06, 1.0 and 3.0 seconds in lattice units

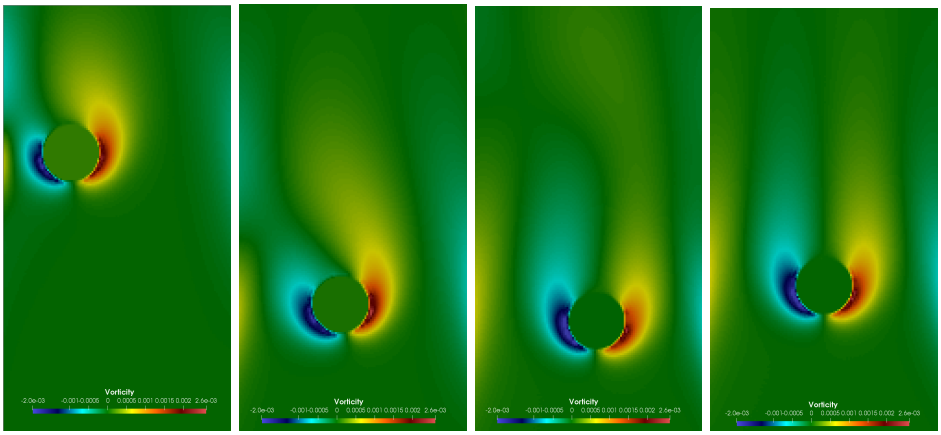

(a) t = 0.4 s (b) t = 0.6 s (c) t = 1.0 s (d) t = 3.0 s

FIGURE 13. Fluid vorticity at times t=0.4, 06, 1.0 and 3.0 seconds in lattice units

method demonstrated its ability to reproduce the complex physics of an airfoil at different angles of attack, and the stall phenomenon was well captured. For this application, the momentum exchange (ME) and stress integration (SI) methods give similar results, but the drag coefficients seem a little more accurate with the SI method. In the second example, a foil oscillating in translation and angle, both methods gave similar results. The complexity of the velocity field is well captured by the two methods used to calculate fluid forces. The final application concerns the sedimentation of particles under the effect of gravity at very low Reynolds numbers. The SI method gave the best results, not least because the extrapolation step in this method smoothes out spurious oscillations in the values of the f_α density function.

However, the trajectories were found perfectly. VP-LBM combined with the stress integration method appears to be a valid tool for simulating fluid-structure interaction problems. At low Reynolds numbers, it is advisable to use the stress integration method, whereas as the Reynolds number increases, the differences between the two methods cancel out, as the influence of the variation in the number of integration points in ME is small. For an extension of the method to three-dimensional cases, the use of the ME should be better. Indeed, the ME method will be easy to use, due to the simplicity of its implementation, whereas the SI method should be expensive, due to the need for a large number of integration points to be placed on the fluid-structure interface, and costly extrapolations on the distribution functions.

REFERENCES

[1] P. Angot, C.-H. Bruneau and P. Fabrie, A penalization method to take into account obstacles in incompressible viscous flows, *Numerische Mathematik*, **81** (1999), 497-520.

[2] M. Benamour, E. Liberge and C. Béghein, Lattice Boltzmann method for fluid flow around bodies using volume penalization, *International Journal of Multiphysics*, **9** (2015), 299-316.

[3] M. Benamour, E. Liberge and C. Béghein, A new approach using lattice Boltzmann method to simulate fluid structure interaction, *Energy Procedia*, **139** (2017), 481-486.

[4] M. Benamour, E. Liberge and C. Béghein, A volume penalization lattice Boltzmann method for simulating flows in the presence of obstacles, *Journal of Computational Science* , **39** (2020), 101050.

[5] R. Benzi, S. Succi and M. Vergassola, The lattice Boltzmann equation: Theory and applications, *Physics Reports*, **222** (1992), 145-197.

[6] P. Bhatnagar, E. Gross and M. Krook, A model for collision processes in gases. I. Small amplitude processes in charged and neutral one-component systems, *Physical Review*, **94** (1954), 511-525.

[7] M. Bouzidi, M. Firdaouss and P. Lallemand, Momentum transfer of a Boltzmann-lattice fluid with boundaries, *Physics of Fluids*, **13** (2001), 3452-3459.

[8] P. Destuynder and E. Liberge, A few remarks on penalty and penalty-duality methods in fluid-structure interactions, *Applied Numerical Mathematics*, **167** (2021), 1-30.

[9] D. d'Humières, Ch. generalized lattice-Boltzmann equations, *Rarefied Gas Dynamics: Theory and Simulations, Progress in Astronautics and Aeronautics*, 1992, 450-458.

[10] G. Di Ilio, D. Chiappini, S. Ubertini, G. Bella and S. Succi, Fluid flow around NACA 0012 airfoil at low-Reynolds numbers with hybrid lattice Boltzmann method, *Computers & Fluids*, **166** (2018), 200-208.

[11] A. Dupuis, P. Chatelain and P. Koumoutsakos, An immersed boundary-lattice-Boltzmann method for the simulation of the flow past an impulsively started cylinder, *Journal of Computational Physics*, **227** (2008), 4486-4498.

[12] Z. Fan, F. Qiu, A. Kaufman and S. Yoakum-Stover, GPU cluster for high performance computing, *IEEE/ACM SC2004 Conference, Proceedings*, (2004), 297-308.

[13] Z.-G. Feng and E. Michaelides, The immersed boundary-lattice Boltzmann method for solving fluid-particles interaction problems, *Journal of Computational Physics*, **195** (2004), 602-628.

[14] J. P. Giovacchini and O. E. Ortiz, Flow force and torque on submerged bodies in lattice-Boltzmann methods via momentum exchange, *Phys. Rev. E*, **92** (2015), 063302.

[15] Z. Guo, C. Zheng and B. Shi, Discrete lattice effects on the forcing term in the lattice Boltzmann method, *Physical Review E*, **65** (2002), 046308.

[16] B. Kadoch, D. Kolomenskiy, P. Angot and K. Schneider, A volume penalization method for incompressible flows and scalar advection-diffusion with moving obstacles, *Journal of Computational Physics*, **231** (2012), 4365-4383.

[17] T. Kinsey and G. Dumas, Parametric study of an oscillating airfoil in a power-extraction regime, *AIAA J.*, **46** (2008), 1318-1330.

[18] T. Kruger, H. Kusumaatmaja, A. Kuzmin, O. Shardt, G. Silva and E. M. Viggen, *The Lattice Boltzmann Method - Principles and Practice*, Graduate Texts in Physics, Springer International Publishing, 2017.

[19] D. F. Kurtulus, On the unsteady behavior of the flow around NACA 0012 airfoil with steady external conditions at re=1000, *International Journal of Micro Air Vehicles*, **7** (2015), 301-326.
[20] A. Ladd and R. Verberg, Lattice-Boltzmann simulations of particle-fluid suspensions, *Journal of Statistical Physics*, **104** (2001), 1191-1251.
[21] H. Li, X. Lu, H. Fang and Y. Qian, Force evaluations in lattice Boltzmann simulations with moving boundaries in two dimensions, *Physical Review E*, **70** (2004), 026701.
[22] Y. Liu, K. Li, J. Zhang, H. Wang and L. Liu, Numerical bifurcation analysis of static stall of airfoil and dynamic stall under unsteady perturbation, *Communications in Nonlinear Science and Numerical Simulation*, **17** (2012), 3427-3434.
[23] D. Noble and J. Torczynski, A lattice-Boltzmann method for partially saturated computational cells, *International Journal of Modern Physics C*, **9** (1998), 1189-1201.
[24] S. Tao, J. Hu and Z. Guo, An investigation on momentum exchange methods and refilling algorithms for lattice Boltzmann simulation of particulate flows, *Computers and Fluids*, **133** (2016), 1-14.
[25] L. Wang, Z. Guo, B. Shi and C. Zheng, Evaluation of three lattice Boltzmann models for particulate flows, *Communications in Computational Physics*, **13** (2013), 1151-1171.
[26] Y. Wang, C. Shu, C. Teo and J. Wu, An immersed boundary-lattice Boltzmann flux solver and its applications to fluid structure interaction problems, *Journal of Fluids and Structures*, **54** (2015), 440-465.
[27] B. Wen, C. Zhang, Y. Tu, C. Wang and H. Fang, Galilean invariant fluid-solid interfacial dynamics in lattice Boltzmann simulations, *Journal of Computational Physics*, **266** (2014), 161-170.
[28] Z. Yang, Lattice Boltzmann outflow treatments: Convective conditions and others, *Computers and Mathematics with Applications*, **65** (2013), 160-171.
[29] D. Yu, R. Mei and W. Shyy, A unified boundary treatment in lattice Boltzmann method, *41st Aerospace Sciences Meeting and Exhibit, AIAA J.*, **1** (2003), 2003-2953.

Received July 2023; revised September 2023; early access October 2023.